Asociación Argentina
de Mecánica Computacional

Mecánica Computacional Vol XXXIII, págs. 909-921 (artículo completo)
Graciela Bertolino, Mariano Cantero, Mario Storti y Federico Teruel (Eds.)
San Carlos de Bariloche, 23-26 Setiembre 2014

CRACKING DEVELOPMENT PREDICTION IN CONCRETE GRAVITY DAMS USING *CONCRETE DAMAGE PLASTICITY MODEL*

María Paula Zappitelli[a], E. Ignacio Villa[a], José Fernández-Sáez[b] and Claudio Rocco[a]

[a] *Departamento de Construcciones, Facultad de Ingeniería, Universidad Nacional de La Plata, Calle 48 y 115 s/n, (B1900TAG) La Plata, Buenos Aires, Argentina. paula.zappitelli@ing.unlp.edu.ar*

[b] *Departamento de Mecánica de Medios Continuos y Teoría de las Estructuras, Universidad Carlos III de Madrid, Av. de la Universidad 30. 29811, Leganés, Madrid, España.*

Keywords: Concrete gravity dam, Concrete Damaged Plasticity, Finite Element Method.

Abstract. As it is well known, many dams around the world are placed in seismic zones. Because of this, it should be check if they can resist dynamic loads typically associated with earthquake occurrences. According to USACE manual (ER 1110-2-2200), modal techniques can be used for dynamic stress analyses in gravity dams, including a simplified response spectrum method and Finite Element Method (FEM), using a response spectrum or acceleration-time record for dynamic input.
In this paper the damage configuration of a concrete gravity dam has been studied. In order to identify the possible crack formation zones a nonlinear model which considers the concrete plastic behavior, was employed to simulate crack propagation within the dam body. The model was numerically implemented in ABAQUS, a FEM analyses code.
The model referred is known as *Concrete Damaged Plasticity*. It assumes that the main two failure mechanisms are tensile cracking and compressive crushing of the concrete material. The evolution of the yield surface is controlled by two hardening variables, ϵ^{pl}_c and ϵ^{pl}_t, linked to failure mechanisms under compression and tension loading, respectively ϵ^{pl}_t becomes u^{pl}_t for non-reinforcement concrete. ϵ^{pl}_c and ϵ^{pl}_t are referred to as compressive and tensile equivalent plastic strains, respectively, while u^{pl}_t is known as "plastic" displacement.
The problem analyzed considers the geometry of Portezuelo del Viento dam, placed in Mendoza, Argentina, in seismic zone 3, according to Argentinian regulation (CIRSOC 103). The design earthquake was described by site-specific accelerations-time records. Prior to the earthquake excitation, the dam is subjected to gravity loading due to its self-weight and to the hydrostatic pressure of the reservoir on the upstream wall.
The results show the damage configuration in the dam, which allow us to identify the possible cracks formation zones and to suggest ways to avoid their development.

1 INTRODUCTION

It is known that many concrete structures, for instance concrete gravity dams, are placed in seismic zones. Engineers should guarantee the good performance of concrete gravity dams along its service life, because the failure of this kind of structures could have catastrophic consequences for human life. For that reason, it should be check if they can resist dynamic loads typically associated with earthquake occurrences. According to USACE manual (ER 1110-2-2200), US Army Corp of Engineers (1995), modal techniques can be used for dynamic stress analyses in gravity dams, including a simplified response spectrum method and Finite Element Method (FEM), using a response spectrum or acceleration-time records for dynamic input.

In order to define the damage configuration in the dam, which allows identifying the possible cracks formation zones, nonlinear models simulating crack propagation within the dam body need to be employed. The nonlinear material behavior of concrete can be realistically simulated by two separate material mechanical processes: damage and plasticity. Plasticity theory has been widely used to describe the concrete behavior. The main characteristic of these models is a yield surface that includes pressure sensitivity, path sensitivity, non-associative flow rule, and work or strain hardening. However, these investigations fail to address the degradation of the material stiffness due to micro-cracking. On the other hand, the continuum damage theory has also been employed to model the material nonlinear behavior such as the mechanical effect of the progressive micro-cracking and strain softening is represented by a set of internal variables at the macroscopic level. The used of coupling between damaged and plasticity has been found to be necessary for capturing the observed experimental-based behavior of concrete, Omidi et al. (2013).

In this paper the damage configuration of the Portezuelo del Viento dam is studied by means of the Concrete Damaged Plasticity Model, available in ABAQUS 6.11, a code by Finite Element Method (FEM). The dam is projected to be placed in Mendoza, Argentina, in seismic zone 3, according to Argentinean regulation, CIRSOC 103 (2013), see Figure 1.

Figure 1: Argentinean seismic zones

The paper is organized as follows. Section 2 explains the framework of the Concrete Damaged Plasticity Model and Section 3 describes the numerical model. In Section 4 the results and their analyses are presented and finally, Section 5 shows the most important conclusions reaches in this paper.

2 THE CONCRETE DAMAGED PLASTICITY MODEL

The *Concrete Damaged Plasticity Model* is a continuum, plasticity-based, damage model for concrete. It assumes that the main two failure mechanisms are tensile cracking and compressive crushing of the concrete material. The evolution of the yield (or failure) surface is controlled by two hardening variables, $\tilde{\varepsilon}_t^{pl}$ and $\tilde{\varepsilon}_c^{pl}$, linked to failure mechanisms under tension and compression loading, respectively. We refer to $\tilde{\varepsilon}_t^{pl}$ and $\tilde{\varepsilon}_c^{pl}$ as tensile and compressive equivalent plastic strains, respectively, ABAQUS (2011).

The model assumes that the uniaxial tensile and compressive response of concrete is characterized by damaged plasticity, as shown in Figure 2.

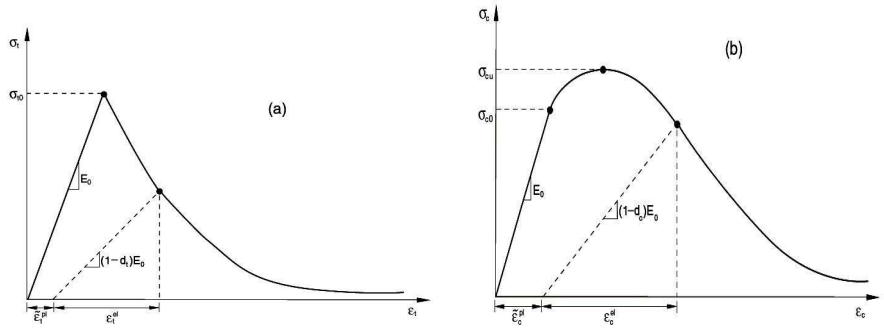

Figure 2: Response of concrete to uniaxial loading in tension (a) and compression (b).

Under uniaxial tension the stress-strain response follows a linear elastic relationship until the value of the failure stress, σ_{t0}, is reached. The failure stress corresponds to the onset of micro-cracking in the concrete material. Beyond the failure stress the formation of micro-cracks is represented macroscopically with a softening stress-strain response, which induces strain localization in the concrete structure. Under uniaxial compression the response is linear until the value of initial yield, σ_{c0}. In the plastic regime the response is typically characterized by stress hardening followed by strain softening beyond the ultimate stress, σ_{cu}, ABAQUS (2011).

It is assumed that the uniaxial stress-strain curves can be converted into stress versus plastic-strain curves using the Eq. (1) and (2):

$$\tilde{\varepsilon}_t^{pl} = \tilde{\varepsilon}_t^{ck} - \frac{d_t}{(1-d_t)}\frac{\sigma_t}{E_0} \tag{1}$$

$$\tilde{\varepsilon}_c^{pl} = \tilde{\varepsilon}_c^{in} - \frac{d_c}{(1-d_c)}\frac{\sigma_c}{E_0} \tag{2}$$

where $\tilde{\varepsilon}_t^{pl}$ y $\tilde{\varepsilon}_c^{pl}$ are equivalent plastic strains in tension and compression, $\tilde{\varepsilon}_t^{ck}$ is the crack strain, $\tilde{\varepsilon}_c^{in}$ is the inelastic strain, d_t and d_c are the damage variable in tension and compression, σ_t and

s_c are the tension and compression stresses and E_0 is the initial undamaged elastic stiffness of the material.

$\tilde{\varepsilon}_t^{ck}$ y $\tilde{\varepsilon}_c^{in}$ are calculated using the Eq. (3) and (4)

$$\tilde{\varepsilon}_t^{ck} = \varepsilon_t - \varepsilon_{0t}^{el} \qquad (3)$$
$$\varepsilon_{0t}^{el} = \sigma_t / E_0$$

$$\tilde{\varepsilon}_c^{in} = \varepsilon_c - \varepsilon_{0c}^{el} \qquad (4)$$
$$\varepsilon_{0c}^{el} = \sigma_c / E_0$$

The damage variables, d_t and d_c, are functions of the plastic strains, the temperature and other file variables. They can take values between 0 and 1.

Considering the former expressions it can conclude that the stress-strain relation under tensile and compressive loads can be written as follows in Eq. (5) and (6):

$$\sigma_t = (1 - d_t) E_0 (\varepsilon_t - \tilde{\varepsilon}_t^{pl}) \qquad (5)$$
$$\sigma_c = (1 - d_c) E_0 (\varepsilon_c - \tilde{\varepsilon}_c^{pl}) \qquad (6)$$

It is important to mention that in the case of unreinforced concrete a stress-displacement curve is employed instead of a stress-strain curve, as it is showed in Figure 3:

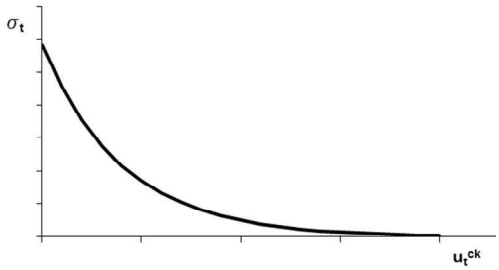

Figure 3: Postfailure stress-displacement curve

The Eq.(7) is used to calculate the “plastic displacements”

$$u_t^{pl} = u_t^{ck} - \frac{d_t}{(1 - d_t)} \frac{\sigma_t l_0}{E_0} \qquad (7)$$

where l_0 is the specimen length and it is assumed to be one unit length.

2.1 Determination of the concrete plasticity parameters

The Concrete Damaged Plasticity Model needs the definition of the flow potential and yield surface parameters. The effective stress is defined as follows in Eq.(8):

$$\bar{\boldsymbol{\sigma}} = \mathbf{D}_0^{el} : (\boldsymbol{\varepsilon} - \boldsymbol{\varepsilon}^{pl}) \tag{8}$$

Where $\bar{\boldsymbol{\sigma}}$ is the effective stress, $\mathbf{D}_0^{el}$ is the initial (undamaged) elasticity matrix, $\boldsymbol{\varepsilon}$ is the total strain and $\boldsymbol{\varepsilon}^{pl}$ is the plastic strain.

The plastic flow potential function and the yield surface make use of two stress invariants of the effective stress tensor, namely the hydrostatic pressure stress and the Misses equivalent effective stress, defined from Eq. (9) and (10):

$$\bar{p} = -\frac{1}{3}\text{trace}\,(\bar{\boldsymbol{\sigma}}) \tag{9}$$

$$\bar{q} = \sqrt{\frac{3}{2}(\bar{\mathbf{S}} : \bar{\mathbf{S}})} \tag{10}$$

where $\bar{\mathbf{S}}$ is the effective stress deviator, defined as follow in Eq. (11):

$$\bar{\mathbf{S}} = \bar{\boldsymbol{\sigma}} + \bar{p}\mathbf{I} \tag{11}$$

The *concrete damaged plasticity model* assumes nonassociated potential plastic flow. The flow potential G used for this model is the Drucker-Prager hyperbolic function, ABAQUS (2011), as it is showed in Eq. (12):

$$G = \sqrt{(\epsilon\sigma_{t0}\tan\psi)^2 + \bar{q}^2} - \bar{p}\tan\psi \tag{12}$$

where $\psi(\theta, f_i)$ is the dilation angle measured in the p–q plane at high confining pressure; $\sigma_{t0}(\theta, f_i) = \sigma_t|_{\tilde{\varepsilon}_t^{pl}=0, \dot{\tilde{\varepsilon}}_t^{pl}=0}$ is the uniaxial tensile stress at failure and $\epsilon(\theta, f_i)$ is a parameter, referred to as the eccentricity, that defines the rate at which the function approaches the asymptote (the flow potential tends to a straight line as the eccentricity tends to zero).

As well the model makes use of the yield function of Lubliner et. al. (1989), with the modifications proposed by Lee and Fenves (1998) to account for different evolution of strength under tension and compression. The evolution of the yield surface is controlled by the hardening variables, $\tilde{\varepsilon}_t^{pl}$ and $\tilde{\varepsilon}_c^{pl}$. In terms of effective stresses, the yield function takes the form of Eq. (13), ABAQUS (2011):

$$F = \frac{1}{1-\alpha}\left(\bar{q} - 3\alpha\bar{p} + \beta(\tilde{\boldsymbol{\varepsilon}}^{pl})\langle\hat{\bar{\sigma}}_{\max}\rangle - \gamma\langle-\hat{\bar{\sigma}}_{\max}\rangle\right) - \bar{\sigma}_c(\tilde{\varepsilon}_c^{pl}) = 0 \tag{13}$$

with:

$$\alpha = \frac{(\sigma_{b0}/\sigma_{c0}) - 1}{2(\sigma_{b0}/\sigma_{c0}) - 1};\ 0 \le \alpha \le 0.5, \tag{14}$$

$$\beta = \frac{\bar{\sigma}_c(\tilde{\varepsilon}_c^{pl})}{\bar{\sigma}_t(\tilde{\varepsilon}_t^{pl})}(1-\alpha) - (1+\alpha) \tag{15}$$

$$\gamma = \frac{3(1-K_c)}{2K_c - 1} \tag{16}$$

where $\hat{\bar{\sigma}}_{\max}$ is the maximum principal effective stress; σ_{b0}/σ_{c0} is the ratio of initial equibiaxial compressive yield stress to initial uniaxial compressive yield stress; K_c is the ratio of the second

stress invariant on the tensile meridian, q(TM), to that on the compressive meridian, q(CM), at initial yield for any given value of the pressure invariant p, such that the maximun principal stress is negative, it must satisfy the condition $0.5 < K_c < 1$; $\bar{\sigma}_t(\tilde{\varepsilon}_t^{pl})$ is the effective tensile cohesion stress and $\bar{\sigma}_c(\tilde{\varepsilon}_c^{pl})$ is the effective compressive cohesion stress.

3 NUMERICAL MODEL

3.1 Overview

In order to study the damage configuration in Portezuelo del Viento dam a 2D model of a dam module was made using a FEM commercial code, ABAQUS V6.11. The dam geometry and dimensions were obtained from Pliego Aprovechamiento Integral del Río Grande Presa y Central Hidroeléctrica Portezuelo del Viento and they can be seen, as well as the FEM mesh, in Figure 4 and 5. Three nodes plane stress triangle elements were used in the model. A nonlinear static and dynamic analysis was performed, and an implicit integration method was used during the simulations.

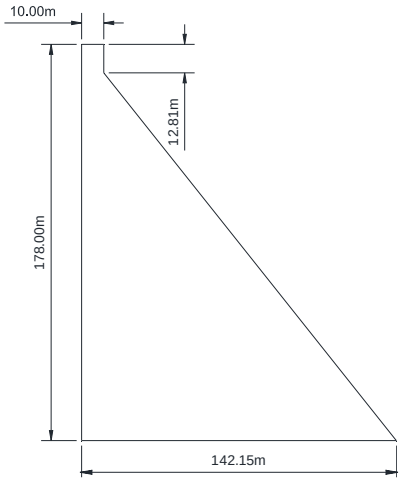

Figure 4: Dam profile analyzed

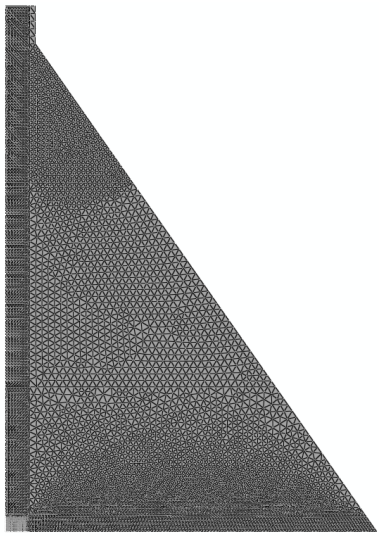

Figure 5: Finite Element Mesh used in the simulation

The load states include gravity loading; hydrostatic pressure produced by a reservoir depth of 175m; hydrodynamic pressure produced by dam-reservoir interaction and ground acceleration in horizontal and vertical directions, see Figure 6.

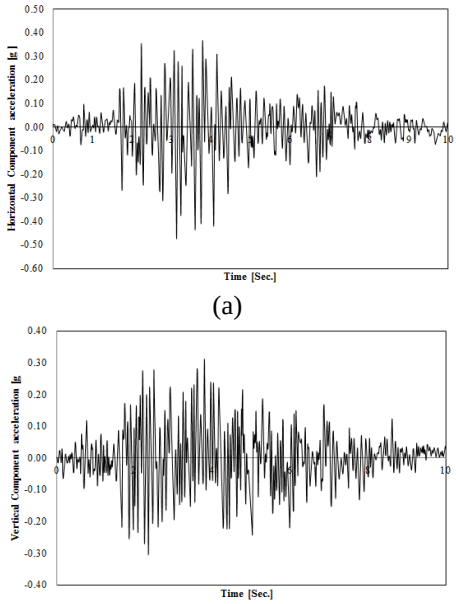

Figure 6: Ground acceleration components of the design earthquake: (a) horizontal, (b) vertical

Dam-reservoir dynamic interactions resulting from the horizontal component of ground motion are included using the Westergaard's method, Westergard (1933). According to Westergaard, the hydrodynamic pressures that the water exerts on the dam during an earthquake are the same as if a certain body of water moves back and forth with the dam while the remainder of the reservoir is left inactive. The added mass per unit area of the upstream wall is given in approximate form by the expression $\frac{7}{8}\rho_w\sqrt{h_w(h_w-y)}$, with $y \leq h_w$, where ρ_w = 1000 kg/m^3 is the density of water.

The hydrodynamic pressures resulting from the vertical component of ground motion are assumed to be small and are neglected in the simulations, ABAQUS (2011). A rigid foundation was assumed in this model.

It is generally accepted that dams have damping ratios of about 2–5%. A 3% fraction of critical damping for the first mode of vibration of the dam was considered in this paper. Assuming Rayleigh stiffness proportional damping, the factor β required to provide a fraction ξ_1 of critical damping for the first mode is given as $\beta = \frac{2\xi_1}{\omega_1}$, ABAQUS (2011) . From a natural frequency extraction analysis of the dam the first eigenfrequency is found to be ω_1= 15.79 rad/ sec. Based on this, β is chosen to be 3.8E^{-3} sec.

3.2 Cases studied

Different dam profiles were analyzed considering three slopes of the downstream wall: 0.7, 0.8 and 0.9. In all cases the influence of the material properties has also been studied, considering three different concretes called C10, C15 and C20, according to CEB recommendations, CEB (1990). Moreover for 0.8 slope dam profile with concrete C15, three

dam heights: 175m, 134m and 89m, corresponding to total height, three quarters of height and a half of height, were considered.

The material properties are shown in Table 1, where the tensile failure stress should be increased by 50% when used with seismic loading to account for rapid loading, US Army Corp of Engineers (1995). The model parameters are: dilation angle (20°), eccentricity (1), relation between biaxial compression and uniaxial compression (1.2) and K factor (0.6666).

To avoid unreasonable mesh-sensitive results due to the lack of reinforcement in the structure, the tensile postfailure behavior is given in terms of a fracture energy cracking criterion by specifying a stress-displacement curve instead of a stress-strain curve, ABAQUS (2011). Similarly, tensile damage, d_t, is specified as a function of cracking displacement. Both curves for concrete C20 are shown in Figure 7. The stiffness degradation damage caused by compressive failure (crushing) of the concrete, d_c, is assumed to be zero.

Concrete		C10	C15	C20	
Density	[Kg/m^3]	2400	2400	2400	-
E	[Pa]	2.62E^{10}	2.84E^{10}	3.03E^{10}	Young´s modulus
n	[-]	0.15	0.15	0.15	Poisson´s ratio
s_{cu}	[Pa]	1.80E^7	2.30E^7	2.80E^7	Compressive ultimate stress
s_{t0}	[Pa]	2.10E^6	2.75E^6	3.33E^6	Tensile failure stress

Table 1: Material properties

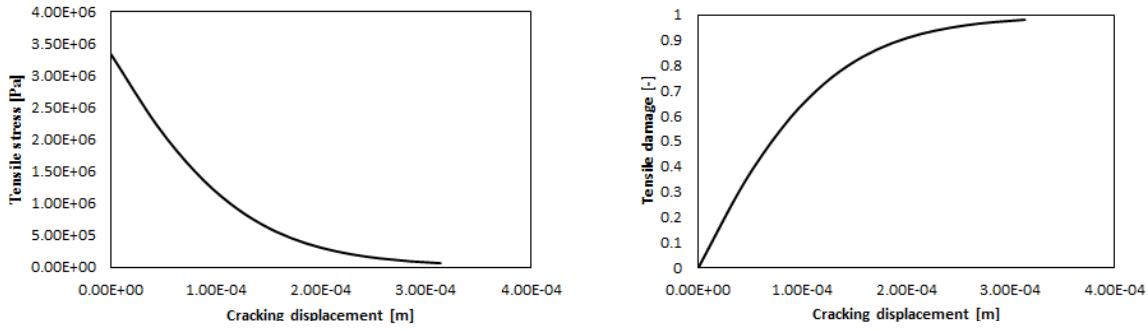

(a) (b)

Figure 7: Concrete tensile properties: (a) tension stiffening and (b) tension damage

4 RESULTS AND ANALYSES

If the changed in the damaged dissipated energy for dams profiles with different slopes and concrete C15 is studied, it can be seen that the higher level of energy is dissipated for the profiles with the highest slope (0.7 in this work), as it is showed in Figure 8 (a). The reason for that behavior is the reduction in the volume of material in profiles with higher slopes.

Figure 8 (b) shows the horizontal displacement at the left corner of the crest for different slopes and concrete C15. Positives values represent displacements in the downstream direction. The profile with the highest slope shows the major displacements, because that profile presents the major level of tensile damage near the dam crest.

Figure 9 (a) shows the damaged dissipated energy for the dam profile slope 0.8 and the three different materials. It can be seen that the major amount of energy is dissipated for concrete C10, because this concrete has the lowest tensile failure stress among the concretes analyzed, so the tensile damage significantly increases in this case.

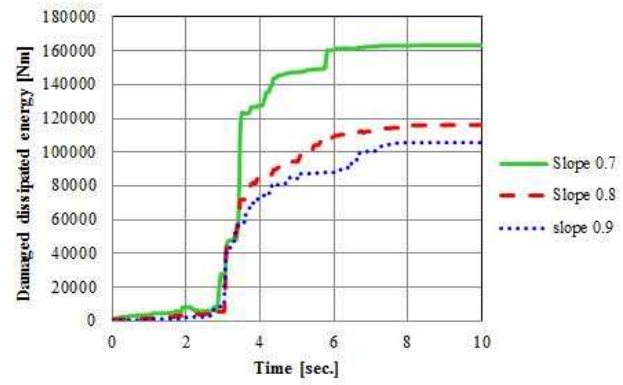

(a)

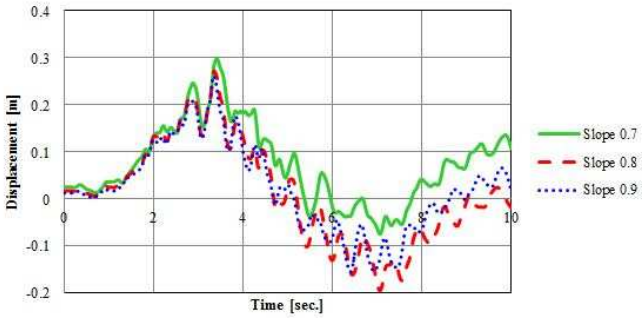

(b)

Figure 8: (a) Damage dissipated energy for different slopes and concrete C15. (b) Displacement at the left corner of the crest for different slopes and concrete C15

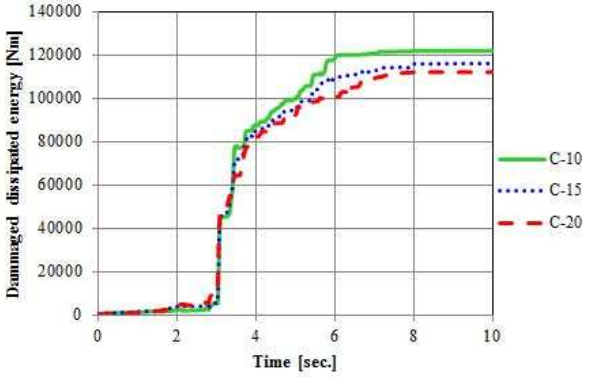

(a)

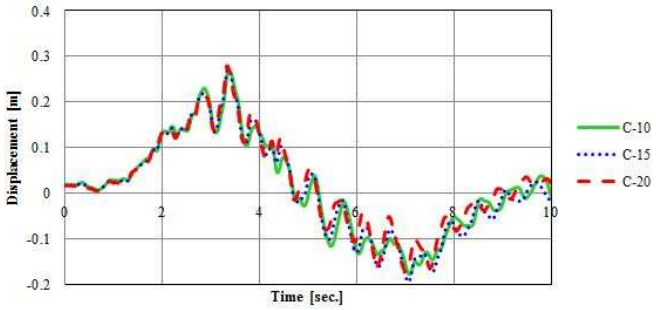

(b)

Figure 9: (a) Damage dissipated energy for different concrete strength and slopes 0.8. (b) Horizontal displacement at the left corner of the dam crest for different concrete strength and slopes 0.8

If the horizontal displacement at the left corner of the dam crest is analyzed it can be shown (see Figure 9 (b)) that the displacements are similar for all the materials studied, but the major values corresponds to concrete C20. The reason for that behavior could be that the tensile damage distribution localized near the dam crest when the concrete strength increases, instead of being distributed in the dam body.

Figure 10 (a) presents the damage dissipated energy for different dam heights (h), concrete C15 and slope 0.8. It can be seen that the major amount of energy is dissipated for the total height (h) and the minor amount correspond to the half of the height. That behaviour can be related to the reduction in the amount of concrete between the cases analyzed.

Horizontal displacement at the left corner of the dam crest is presented in Figure 10 (b) for different dam heights. As it can be expected the longer displacements correspond to the total height (h), which can be related to the fact that at upper heights the earthquake effects are stronger because the structure is far from the basement constraints.

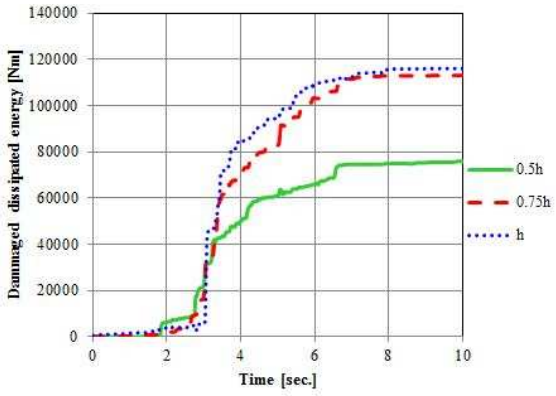

(a)

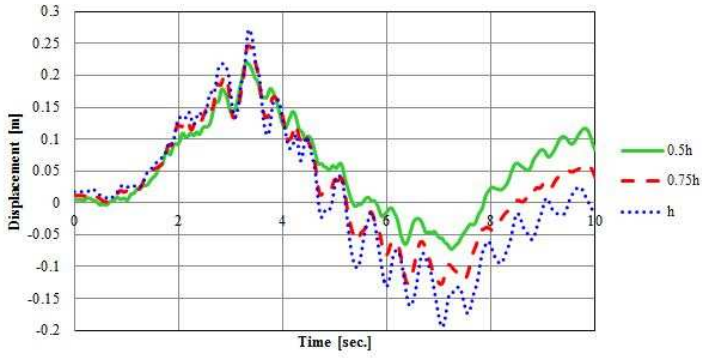

(b)

Figure 10: (a) Damage dissipated energy for different dam heights, concrete C15 and slope 0.8. (b) Horizontal displacement at the left corner of the dam crest for different dam heights, concrete C15 and slope 0.8

Figure 11 shows the earthquake horizontal acceleration component together with the damaged dissipated energy speed for concrete C15 and dam profile slope 0.8. It could be seen that the highest damage dissipated energy speed values take place during the highest acceleration levels, between 3 and 5 seconds.

As it can be seen in Figure 12, the tensile damage grows in that period of time and after that it keeps without increasing significantly. The tensile damage is measured using the variable DAMAGET available in ABAQUS 6.11, which takes values between 0 and 1, where 1 represents complete damage. The damage initiates at the dam heel at the end of the hydrostatic step, it continues growing at the dam heel during the dynamic step, after that it initiates in the upstream face and continues in the downstream face.

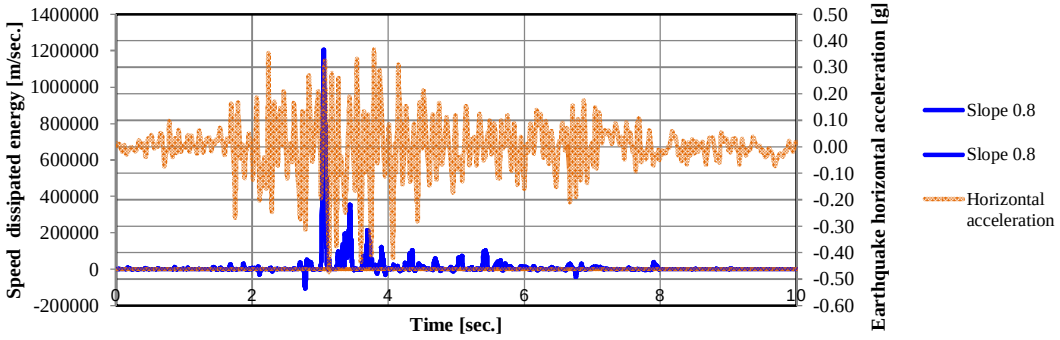

Figure 11: Earthquake horizontal acceleration component overlapped the damage dissipated energy speed for concrete C15 and dam profile slope 0.8

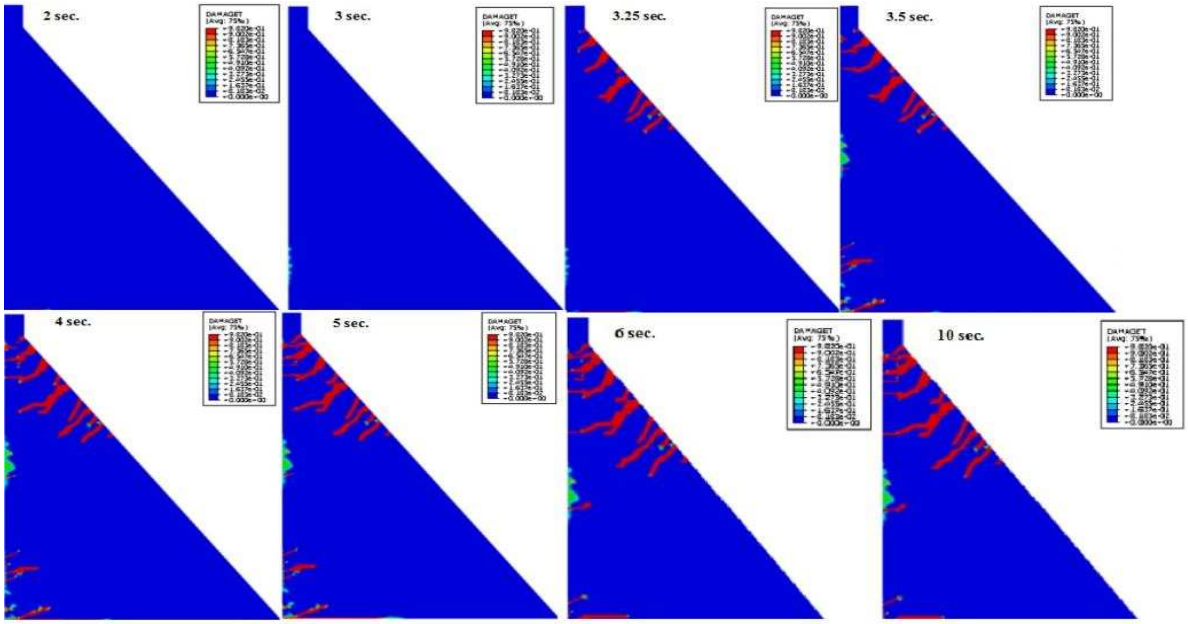

Figure 12: Tensile damaged configuration for slope 0.8 and concrete C15

5 SUMARY AND CONCLUSIONS

In this paper the damaged configuration of *Portezuelo del Viento* dam profile was studied considering three slopes of the downstream wall: 0.7, 0.8 and 0.9, and in all cases the influence of the material properties have also been studied, by considering three different concretes called C10, C15 and C20. The effect of the dam height for 0.8 slope and concrete C15 was also studied. A model known as *Concrete Damaged Plasticity* available in ABAQUS 6.11, that considers the concrete plastic behavior was used. Prior to the earthquake excitation, the dam is subjected to gravity loading due to its self-weight and to the hydrostatic pressure of the reservoir on the upstream wall.

It can be concluded that the major tensile damage takes place for higher profile slope (0.7) and lower concrete tensile failure stress (C10). In this case the tensile damage grows during a short time period, about 2 seconds, and after that period it keeps without growing significantly. This is important because energy dissipation mechanisms should be applied during this time period to reduce the damage level.

If different dam heights for the same slope (0.8) and concrete (C10) are compared, it can be seen that the major damage and crest displacements take place for upper heights (h), which can be related to the distance to the basement constraints.

REFERENCES

US Army Corp of Engineers, Gravity dam desing. EM 1110-2-2200. 30 June 1995.

Omidi, O.; Valliappan, S.; Lotfi, V., Seismic cracking of concrete gravity dams by plastic-damage model using different damping mechanisms. *In: Finite Elements in Analysis and Desing* (2013) No. 63, pp. 80-97.

Reglamento INPRES-CIRSOC 103: Reglamento Argentino para Construccines Sismoresistentes. Parte I. Construcciones en general. Septiembre 2013.

Dassault Systèmes Simulia Corp.: ABAQUS. User's Manual Version 6.11 (2011) Vol. 3, pp 437-465.

Lubliner, J., J. Oliver, S. Oller, and E. Oñate, A Plastic-Damage Model for Concrete, *International Journal of Solids and Structures*, vol. 25, pp. 299–329, 1989.

Lee, J., and G. L. Fenves, Plastic-Damage Model for Cyclic Loading of Concrete Structures, *Journal of Engineering Mechanics*, vol. 124, no. 8, pp. 892–900, 1998.

Gobierno de la provincia de Mendoza, Ministerio de Infraestructura, Vivienda y Transporte, Secretaría de Obras Públicas: Pliego Aprovechamiento Integral del Río Grande Presa y Central Hidroeléctrica Portezuelo del Viento.

Westergaard, H. M., Water Pressures on Dams during Earthquakes. *Transactions of the American Society of Civil Engineers* (1933) Vol 98, pp 418-433.

Dassault Systèmes Simulia Corp.: ABAQUS. Example problems Manual Version 6.11 (2011) Vol 1, pp 733-746.

CEB-FIB: Model Code 1990. Parte I. June 1991.